Rayleigh scattering of surface plasmons by sub-wavelength holes

F. van Beijnum,[1] **A.S. Meeussen,**[1] **C. Rétif,**[2] **and M.P. van Exter,**[1,*]

[1] *Huygens Laboratory, Leiden University, PO Box 9504, 2300 RA Leiden, The Netherlands*

[2] *FOM Institute for Atomic and Molecular Physics, Science Park 104, 1098 XG Amsterdam, The Netherlands*

** exter@physics.leidenuniv.nl*

Abstract: We study the scattering of surface plasmons from sub-wavelength holes and find that it exhibits a stronger wavelength dependence than the traditional λ^{-4} scaling found for Rayleigh scattering of light from small particles. This experimental observation is consistent with recent theoretical work and linked to the two-dimensional nature of the surface plasmon and the wavelength dependence of its spatial extent in the third dimension. The scattering cross sections are obtained with a frequency-correlation technique, which compares intensity speckle patterns observed behind various random structures of holes and recorded at different wavelengths. This powerful technique even allows us to distinguish between scattering of surface plasmons into photons and scattering into other surface plasmons.

OCIS codes: (240.6680) Surface plasmons, (290.5870) Rayleigh Scattering.

References and links

1. S. Zhang, W. Fan, N. C. Panoiu, K. J. Malloy, R. M. Osgood, and S. R. J. Brueck, "Experimental Demonstration of Near-Infrared Negative-Index Metamaterials," Phys. Rev. Lett. **95**, 137404 (2005).
2. J. Valentine, J. Li, T. Zentgraf, G. Bartal, and X. Zhang, "An optical cloak made of dielectrics," Nature Mater. **8**, 568–571 (2009).
3. L. Sapienza, H. Thyrrestrup, S. Stobbe, P. D. Garcia, S. Smolka, and P. Lodahl, "Cavity Quantum Electrodynamics with Anderson-Localized Modes," Science **327**, 1352–1355 (2010).
4. A. G. Brolo, "Plasmonics for future biosensors," Nature Photon. **6**, 709–713 (2012).
5. K. Vynck, M. Burresi, F. Riboli, and D. S. Wiersma, "Photon management in two-dimensional disordered media," Nature Mater. **11**, 1017–1022 (2012).
6. T. W. Ebbesen, H. J. Lezec, H. F. Ghaemi, T. Thio, and P. A. Wolff, "Extraordinary optical transmission through sub-wavelength hole arrays," Nature **391**, 667–669 (1998).
7. H. A. Bethe, "Theory of Diffraction by Small Holes," Phys. Rev. Online Archive (Prola) **66**, 163–182 (1944).

#203316 - $15.00 USD Received 17 Dec 2013; revised 14 Feb 2014; accepted 17 Feb 2014; published 22 Apr 2014

8. F. J. García-Vidal, L. Martín-Moreno, T. W. Ebbesen, and L. Kuipers, "Light passing through subwavelength apertures," Rev. of Mod. Phys. **82**, 729–787 (2010).
9. J. M. Yi, A. Cuche, de León Pérez, A. Degiron, E. Laux, E. Devaux, C. Genet, J. Alegret, L. M. Moreno, and T. W. Ebbesen, "Diffraction Regimes of Single Holes," Phys. Rev. Lett. **109**, 023901 (2012).
10. K. L. van der Molen, K. J. Klein Koerkamp, S. Enoch, F. B. Segerink, N. F. van Hulst, and L. Kuipers, "Role of shape and localized resonances in extraordinary transmission through periodic arrays of subwavelength holes: Experiment and theory," Phys. Rev. B **72**, 045421 (2005).
11. T. Matsui, A. Agrawal, A. Nahata, and Z. V. Vardeny, "Transmission resonances through aperiodic arrays of subwavelength apertures," Nature **446**, 517–521 (2007).
12. J. W. Lee, M. A. Seo, D. H. Kang, K. S. Khim, S. C. Jeoung, and D. S. Kim, "Terahertz Electromagnetic Wave Transmission through Random Arrays of Single Rectangular Holes and Slits in Thin Metallic Sheets," Phys. Rev. Lett. **99**, 137401 (2007).
13. F. van Beijnum, C. Rétif, C. B. Smiet, and M. P. van Exter, "Transmission processes in random patterns of subwavelength holes," Opt. Lett. **36**, 3666–3668 (2011).
14. F. Przybilla, C. Genet, and T. W. Ebbesen, "Long vs. short-range orders in random subwavelength hole arrays," Opt. Express **20**, 4697–4709 (2012).
15. L. Yin, V. K. Vlasko-Vlasov, J. Pearson, J. M. Hiller, J. Hua, U. Welp, D. E. Brown, and C. W. Kimball, "Subwavelength Focusing and Guiding of Surface Plasmons," Nano Lett. **5**, 1399–1402 (2005).
16. A. Y. Nikitin, F. J. García-Vidal, and L. Martín-Moreno, "Surface Electromagnetic Field Radiated by a Subwavelength Hole in a Metal Film," Phys. Rev. Lett. **105**, 073902 (2010).
17. A. V. Shchegrov, I. V. Novikov, and A. A. Maradudin, "Scattering of Surface Plasmon Polaritons by a Circularly Symmetric Surface Defect," Phys. Rev. Lett. **78**, 4269–4272 (1997).
18. N. Rotenberg, M. Spasenović, T. L. Krijger, B. L. Feber, F. J. G. de Abajo, and L. Kuipers, "Plasmon Scattering from Single Subwavelength Holes," Phys. Rev. Lett. **108**, 127402 (2012).
19. H. T. Liu and P. Lalanne, "Microscopic theory of the extraordinary optical transmission," Nature **452**, 728–731 (2008).
20. F. van Beijnum, C. Retif, C. B. Smiet, H. Liu, P. Lalanne, and M. P. van Exter, "Quasi-cylindrical wave contribution in experiments on extraordinary optical transmission," Nature **492**, 411–414 (2012).
21. J. W. Strutt, "XV. On the light from the sky, its polarization and colour," Phil. Mag. Series 4 **41**, 107–120 (1871).
22. D. S. Kim, S. C. Hohng, V. Malyarchuk, Y. C. Yoon, Y. H. Ahn, K. J. Yee, J. W. Park, J. Kim, Q. H. Park, and C. Lienau, "Microscopic Origin of Surface-Plasmon Radiation in Plasmonic Band-Gap Nanostructures," Phys. Rev. Lett. **91**, 143901 (2003).
23. J. Li, H. Iu, D. Y. Lei, J. T. K. Wan, J. B. Xu, H. P. Ho, M. Y. Waye, and H. C. Ong, "Dependence of surface plasmon lifetimes on the hole size in two-dimensional metallic arrays," Appl. Phys. Lett. **94**, 183112 (2009).
24. P. Yeh, *Optical waves in layered media* (Wiley, New York, 1998).
25. F. van Beijnum, J. Sirre, C. Rétif, and M. P. van Exter, "Speckle correlation functions applied to surface plasmons," Phys. Rev. B **85**, 035437 (2012).
26. S. Feng, C. Kane, P. A. Lee, and A. D. Stone, "Correlations and Fluctuations of Coherent Wave Transmission through Disordered Media," Phys. Rev. Lett. **61**, 834–837 (1988).
27. I. Freund, M. Rosenbluh, and S. Feng, "Memory Effects in Propagation of Optical Waves through Disordered Media," Phys. Rev. Lett. **61**, 2328–2331 (1988).
28. M. P. van Albada, B. A. van Tiggelen, A. Lagendijk, and A. Tip, "Speed of propagation of classical waves in strongly scattering media," Phys. Rev. Lett. **66**, 3132–3135 (1991).
29. R. Berkovits and S. Feng, "Correlations in coherent multiple scattering," Phys. Reports **238**, 135–172 (1994).
30. S. Faez, P. M. Johnson, and A. Lagendijk, "Varying the Effective Refractive Index to Measure Optical Transport in Random Media," Phys. Rev. Lett. **103**, 053903 (2009).
31. J. Bertolotti, E. G. van Putten, C. Blum, A. Lagendijk, W. L. Vos, and A. P. Mosk, "Non-invasive imaging through opaque scattering layers," Nature **491**, 232–234 (2012).

#203316 - $15.00 USD Received 17 Dec 2013; revised 14 Feb 2014; accepted 17 Feb 2014; published 22 Apr 2014

32. P. Lalanne and J. P. Hugonin, "Interaction between optical nano-objects at metallo-dielectric interfaces," Nature Phys. **2**, 551–556 (2006).
33. A. Y. Nikitin, S. G. Rodrigo, F. J. García-Vidal, and L. Martín-Moreno, "In the diffraction shadow: Norton waves versus surface plasmon polaritons in the optical region," New Journal of Physics **11**, 123020 (2009).
34. W. Dai and C. M. Soukoulis, "Theoretical analysis of the surface wave along a metal-dielectric interface," Phys. Rev. B **80**, 155407 (2009).
35. P. B. Johnson and R. W. Christy, "Optical Constants of the Noble Metals," Phys. Rev. B **6**, 4370–4379 (1972).
36. E. D. Palik, *Handbook of Optical Constants of Solids* (Academic Press, 1985).
37. R. E. Thomas and G. A. Haas, "Diffusion measurements in thin films utilizing work function changes: Cr into au," J. of Appl. Phys. **43**, 4900–4907 (2003).
38. M. Rost, D. Quist, and J. Frenken, "Grains, growth, and grooving," Phys. Rev. Lett. **91** (2003).
39. N. Rotenberg, T. L. Krijger, B. L. Feber, M. Spasenović, F. J. G. de Abajo, and L. Kuipers, "Magnetic and electric response of single subwavelength holes," Phys. Rev. B **88**, 241408(R) (2013).
40. L. Novotny and B. Hecht, *Principles of Nano-Optics* (Cambridge University Press, 2006).
41. H.C. van de Hulst, *Light Scattering by Small Particles* (Dover, 1985).

1. Introduction

Sub-wavelength holes are important building blocks for novel photonic structures, given that these holes are used in metamaterials [1, 2], photonic crystal slabs [3], sensors [4] and possibly thin film solar cells [5]. In the context of the extraordinary optical transmission [6], the transmission of light through single sub-wavelength holes in metal films has attracted much interest and its physics is surprisingly rich [7–9]. To measure this single hole transmission, random patterns of sub-wavelength holes can be used [10–14]

The excitation [15, 16] and scattering [17, 18] of surface plasmons by single sub-wavelength holes has been studied both theoretically and experimentally. The wavelength dependence of these scattering processes, which play a central role in recently developed microscopic models [19, 20], can reveal the underlying physics of surface plasmon scattering. So far, this wavelength dependence has only been studied using metal hole arrays. One study reports the traditional [21] $1/\lambda^4$ dependence [22], while another study reports a λ^{-n} wavelength dependence where the power n depends strongly on hole size [23]. Both experimental observations contradict theories on surface plasmon scattering [17, 18].

For surface plasmons scattered at a single hole, the scattering cross section has unit length instead of an area [17,18]. This is because the cross section is the scattered power divided by the incident power in the plasmon mode *per unit width*, measured along the surface and perpendicular to the propagation direction [17, 18, 24]. Because the scattering cross section for surface plasmons has unit length, the traditional expression [21] of λ^{-4} times a volume squared can not be correct.

In this letter we extract the Rayleigh scattering cross sections of surface plasmons from single sub-wavelength holes by studying the optical transmission of random patterns of holes. An advantage of using random patterns is that most interference effects can be averaged, in contrast to the transmission of arrays which is entirely dominated by interference effects. Another important advantage of random patterns is that they

#203316 - $15.00 USD Received 17 Dec 2013; revised 14 Feb 2014; accepted 17 Feb 2014; published 22 Apr 2014

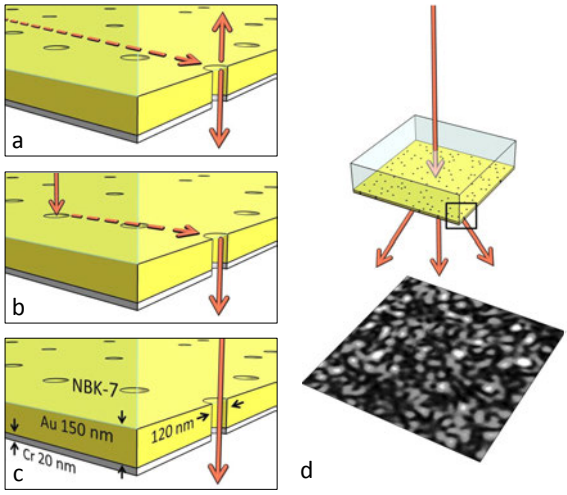

Fig. 1. (a-c) Our experiments probe three scattering processes: (a) Coupling of a surface plasmon to free space via scattering at a single hole; (b) Surface-plasmon-mediated transmission, where a surface plasmon is first excited at one hole and then transmitted at another hole; (c) Direct transmission through a sub-wavelength hole. (d) Random patterns of sub-wavelength holes are illuminated by a spectrally filtered supercontinuum laser source, of which we scan the wavelength. The change of the speckle pattern as a function of wavelength difference $\Delta\lambda$ is quantified by calculating the correlation $C(\Delta\lambda)$.

enable us to separate (ohmic) absorption from (radiative) scattering loss, by comparing samples of different hole densities [25].

Figure 1 (a-c) show the three physical processes that we probe: (a) scattering of surface plasmons to free space, (b) surface-plasmon-mediated optical transmission, and (c) direct transmission. Figure 1(d) shows a sketch of the experiment. This experiment yields three quantities: the surface plasmon absorption length L_{abs}, the scattering cross section σ, and a new concept that we name the intensity-ratio cross section A. The surface plasmon absorption length L_{abs} quantifies the ohmic loss of the surface plasmons. The scattering cross section σ characterizes the radiative loss of a surface plasmon at a single hole (Fig. 1(a)); it singles out the scattering to free space and is insensitive to scattering within the surface plasmon manifold. The intensity-ratio cross section A describes the transmission of light via a surface plasmon, where a surface plasmon is first excited at one hole and then transmitted at another hole (Fig. 1(b)). This cross section is approximately equal to, but slightly smaller than, the scattering cross section from surface plasmons to surface plasmons, such that $A = \eta\sigma_{spp}$ with $\eta \approx 1$ (see below). Before presenting the wavelength dependence of L_{abs}, σ and A, we will first show how we extract these quantities from the optical transmission of random patterns of holes.

#203316 - $15.00 USD Received 17 Dec 2013; revised 14 Feb 2014; accepted 17 Feb 2014; published 22 Apr 2014

2. Experiment

Our experiments are performed on a series of random patterns of sub-wavelength holes in a metal film. The series contains 8 patterns of which only the hole density was varied. We choose the area per hole (= inverse hole density) to be qa_0^2, with $a_0 = 0.45\ \mu$m and $q \in [1,2,3,4,9,16,25,36]$. The circular holes (diameter of 140 ± 8 nm) perforate a 150 nm thick gold film, which is deposited directly on glass omitting the commonly used adhesion layer. A subsequently deposited 20 nm chromium layer damps the surface plasmons on the gold-air interface, allowing us to selectively study surface plasmons on the gold-glass interface (see Fig. 1(c)). The random pattern is generated using a random number generator that generates the coordinates of the holes one by one. When new holes almost (< 50 nm) overlap existing holes, they are placed at new random positions instead.

We illuminate these random patterns of sub-wavelength holes with monochromatic light and record the far-field speckle intensity $I(\vec{\theta},\lambda)$ (see Fig. 1(d)). The change of the speckle pattern with wavelength can be quantified by calculating the correlation between the measured speckle intensity at wavelengths λ_0 and $\lambda_1 = \lambda_0 + \Delta\lambda$, resulting in a correlation function $C(\Delta\lambda)$ [25–31]. More precisely, we compare intensities at the same transverse momentum $\vec{k}_{||} = 2\pi/\lambda(\sin\theta_x, \sin\theta_y)$, which is achieved experimentally by rescaling the recorded speckle patterns [25]. We perform these measurements in a large wavelength range using a supercontinuum laser source (Fianum Whitelase 400SC) of which we select a narrow line (~ 1 nm) with a spectrometer.

Using a simple model, which assumes that only surface plasmons (SP) are excited at the holes and thus neglects the quasi-cylindrical wave contribution [32–34], we find an analytic expression for the correlation function [25]:

$$C(\Delta\lambda) = \frac{1}{\langle I_d + I_s\rangle^2}\left|\langle I_d\rangle + \frac{\langle I_s\rangle}{1 - iL_{\mathrm{tot}}\,\mathrm{Re}\,[\Delta k_{\mathrm{spp}}]}\right|^2. \tag{1}$$

Equation (1) contains two density-dependent parameters: L_{tot}, the propagation distance of the surface plasmons, which includes both radiative and non-radiative losses, and the intensity ratio $\langle I_s\rangle / \langle I_d\rangle$ between the intensities of the SP-mediated and direct transmission. The term $\mathrm{Re}\,[\Delta k_{\mathrm{spp}}]$ is the difference between the surface plasmon momenta at wavelengths λ_0 and λ_1. It can be approximated by $\mathrm{Re}\,[\Delta k_{\mathrm{spp}}] \approx 2\pi\,\mathrm{Re}\,n_{\mathrm{eff}}\Delta\lambda/\bar{\lambda}^2$, with n_{eff} the effective refractive index of the surface plasmon mode and $\bar{\lambda}$ the average wavelength in vacuum. Equation (1) is a Lorentzian with an almost wavelength-independent background correlation $\langle I_d\rangle^2 / \langle I_d + I_s\rangle^2$.

Figure 2 shows three examples of measured correlation functions (on a log-linear scale) for three different hole densities. The scans in this plot are performed from $\lambda =$ 690 nm ($\Delta\lambda = 0$ nm) to 790 nm ($\Delta\lambda = 100$ nm). With increasing hole density the background correlation, visible at large $\Delta\lambda$, decreases while the spectral width of the correlation increases. The observation that the background correlation decreases shows that the efficiency of transmission via surface plasmons increases with density, as a larger fraction of the excited surface plasmons is coupled out instead of being absorbed.

#203316 - $15.00 USD Received 17 Dec 2013; revised 14 Feb 2014; accepted 17 Feb 2014; published 22 Apr 2014

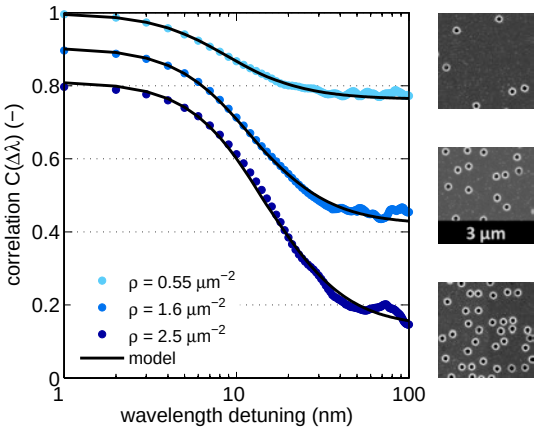

Fig. 2. The measured correlation functions $C(\Delta\lambda)$ have a wavelength-dependent contribution, caused by surface plasmons propagating on the gold-glass interface, and a wavelength-independent contribution resulting from light that is directly transmitted through the holes. The correlation functions depend strongly on hole density: the width increases with density while the background decreases. For the clarity of the figure, the plots for $\rho = 1.6\ \mu\text{m}^2$ and $\rho = 2.5\ \mu\text{m}^2$ are offset by -0.1 and -0.2 respectively.

This increase in outcoupling is also evidenced by the increasing spectral width, which is directly related to the losses of the surface plasmons.

The three fits in Fig. 2 are based on Eq. (1) and in good correspondence with the data. From each fit two density-dependent parameters can be extracted: L_{tot} and $\langle I_s \rangle / \langle I_d \rangle$. Figure 3(a) shows the density dependence of L_{tot}, not only for the correlation measurements starting from $\lambda_0 = 690$ nm, which is labeled with the average wavelength $\bar{\lambda} = 705 \pm 15$ nm, but also for $\bar{\lambda} = 803 \pm 13$ nm and 881 ± 9 nm. Each of these sets of results obeys the expected relation:

$$L_{\text{tot}}^{-1}(\rho) = L_{\text{abs}}^{-1} + \rho\sigma, \tag{2}$$

where L_{abs} is the surface plasmon absorption length in the absence of the holes and σ is a scattering cross section that describes the radiative loss of a surface plasmon at a single hole. For $\bar{\lambda} = 705 \pm 15$ nm we thus obtain the (density-independent) inverse absorption length $L_{\text{abs}} = 0.20 \pm 0.02\ \mu\text{m}^{-1}$ and the scattering cross section $\sigma = 80 \pm 15$ nm. For the two other wavelengths, we find a similar linear dependence $L_{\text{tot}}^{-1}(\rho) = L_{\text{abs}}^{-1} + \rho\sigma$, but with different slopes and different axis cutoffs. The slope σ decreases by as much as a factor four between $\bar{\lambda} = 705 \pm 15$ nm and 803 ± 13 nm, and almost vanishes at $\bar{\lambda} = 881 \pm 9$ nm. The axis cutoff L_{abs}^{-1} decreases with wavelength by more than a factor two over this wavelength range. Both observations are consistent with the theoretically expected dependence. They will be discussed in the next section, where we will combine them with similar results obtained at other wavelengths.

The second parameter that we obtain from the correlation functions is the intensity

#203316 - $15.00 USD Received 17 Dec 2013; revised 14 Feb 2014; accepted 17 Feb 2014; published 22 Apr 2014

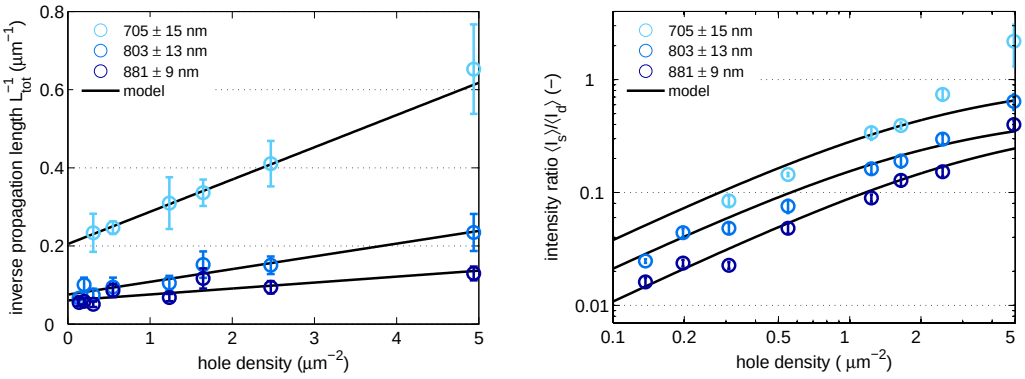

Fig. 3. (a, left) The inverse propagation length L_{tot}^{-1} as a function of density for three different wavelength ranges. Both the axis cutoff, i.e. the absorption, and the slope decrease with wavelength. (b, right) The density dependence of the intensity ratio $\langle I_s \rangle / \langle I_d \rangle$. For each density the intensity ratio decreases with wavelength. In the low density regime the intensity ratio increases linearly.

ratio $\langle I_s \rangle / \langle I_d \rangle$. In Fig. 3(b) we show the density dependence of the obtained intensity ratio and compares it with the expected dependence [25]:

$$\frac{\langle I_s \rangle}{\langle I_d \rangle}(\rho) = \frac{A\rho}{\rho\sigma + L_{\mathrm{abs}}^{-1}}, \tag{3}$$

where A is the third density-independent parameter, which we name the intensity-ratio cross section. Equation (3) provides a good fit of the experimental data, using only A as a free parameter, in combination with the values of L_{abs} and σ obtained from the fit of Fig. 3(a). Figure 3(b) also shows a signature of the quasi-cylindrical wave, as the intensity ratio for the largest density is consistently larger than predicted by our model. For this reason we limited our analysis to hole densities smaller than 2.5 μm^2. A comparison of the fitted values of A at the three wavelengths ($\bar{\lambda} = 705, 803, 881$ nm) shows that the wavelength dependence of this parameter is even slightly stronger than that of the scattering cross section σ. It will be discussed in the next section.

To summarize this section, we have measured the correlation functions $C(\Delta\lambda)$ of samples with different hole densities and fitted these with Eq. 1, using two *density-dependent* parameter: the SP propagation length $L_{\mathrm{tot}}(\rho)$ and the intensity ratio $\langle I_s \rangle / \langle I_d \rangle$ (ρ). Next, we analyze the ρ-dependence of these parameter in order to extract three *density-independent* parameters: the absorption length L_{abs}, the scattering cross section σ, and the intensity-ratio cross section A. By performing this analysis for different values of the reference wavelength λ_0, we also find the wavelength dependence of these parameters. In the rest of the paper, we try to understand the wavelength dependence of L_{abs} and the scattering parameters σ and A, using Rayleigh scattering of surface plasmons at single holes as microscopic model.

#203316 - $15.00 USD Received 17 Dec 2013; revised 14 Feb 2014; accepted 17 Feb 2014; published 22 Apr 2014

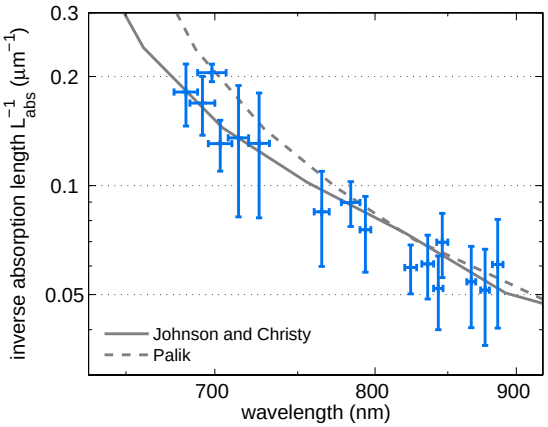

Fig. 4. Inverse absorption length L_{abs}^{-1} as a function of wavelength, as extracted from our experiments. The obtained absorption length is in good agreement with theory, showing both the validity of our experiment and the quality of the gold layer. The error in wavelength corresponds to the characteristic spectral width of the correlation function of the low density samples, and is therefore smaller for larger wavelengths

3. Results

In Fig. 4 we show the measured wavelength dependence of the absorption length L_{abs} to the power -1. This length increases by approximately a factor four from $L_{\text{abs}} \approx 5\ \mu$m to $L_{\text{abs}} \approx 20\ \mu$m, when the wavelength is increased from 650 nm to 950 nm. The data matches very well with the theory for which we use literature values of the refractive index of gold [35, 36]. This correspondence is very important as it demonstrates the validity of our approach, both qualitative and quantitative.

In Fig. 5(a) we plot the extracted value for the scattering cross section σ as a function of wavelength. This cross section shows a steep decline from slightly more than 100 nm at a wavelength of 675 nm to around 15 nm at 875 nm. This decline is significantly steeper than the traditional expression for Rayleigh scattering ($\sigma \propto \lambda^{-4}$) indicated by the dashed line.

Recently, an analytic expression was derived for the scattering cross section of surface plasmons scattered at a sub-wavelength hole [18]. This theory treats the hole as a polarizable object, relative to its surroundings, and distinguished between scattering to other surface plasmons and to photons. For surface plasmons scattered to the photon field this expression is (see Appendix A):

$$\sigma = \xi \frac{k^4 a^6}{d_{spp}} \tag{4}$$

where a is the hole radius, k is the wave vector in air, d_{spp} is the mode size of the surface plasmon. The dimensionless proportionality constant ξ is radius independent in the Rayleigh limit, i.e. for $ka \ll 1$. Hence, the expression for surface-plasmon scattering

#203316 - $15.00 USD Received 17 Dec 2013; revised 14 Feb 2014; accepted 17 Feb 2014; published 22 Apr 2014

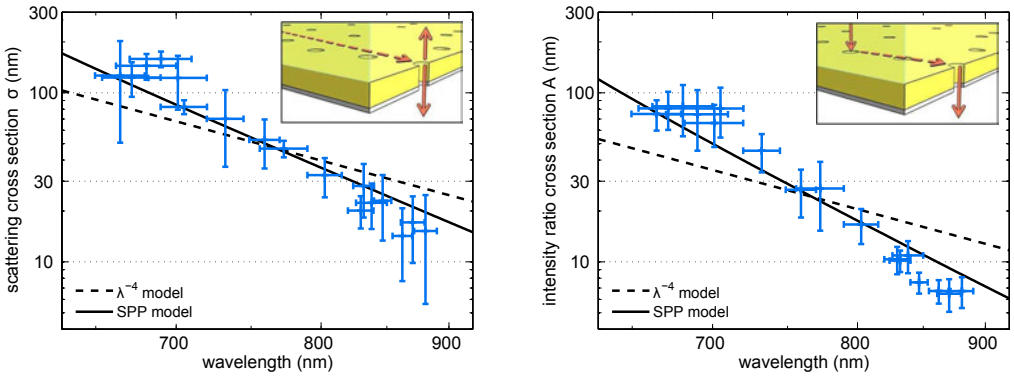

Fig. 5. (a, left) The scattering cross section σ, which describes the radiative loss of a surface plasmon at a single hole, decreases almost a factor 10 in the measured wavelength range. (b, right) The intensity-ratio cross section A quantifies the transmission of light via a surface plasmon, by excitation at one hole and scattering and transmission at another hole. This parameter also decreases almost a factor 10 in the measured wavelength range and is comparable in magnitude to the scattering cross section σ. The error in wavelength corresponds to the spectral width of the correlation functions for high density samples

resembles the expression $\sigma_{3D} \propto k^4 a^6$ for the scattering of light by three dimensional particles, but the surface-plasmon mode size d_{spp} enters as a proportionality factor. This factor indicates that the hole is polarized more effectively when the surface plasmon mode is more compact. For our experiments d_{spp} is well approximated by the 1/e width of the intensity tail in the dielectric. For surface plasmons at a metal-air interface we find $d_{spp} \approx \sqrt{|\varepsilon|}/(2k)$, with ε the dielectric constant of the metal (assuming $|\varepsilon| \gg 1$). At sufficiently large wavelength, where the Drude result $|\varepsilon| = |\varepsilon_\infty - b/k^2| \propto k^{-2}$ applies, we thus expect $d_{spp} \propto k^{-2}$ and $\sigma \propto k^6$. For accurate fitting, we use the literature values of ε [36], rather than the Drude approximation.

The solid curve in Fig. 5(a) shows that Eq. (4) fits the data much better than the ordinary Rayleigh scaling $\sigma \propto \lambda^{-4}$. This is a very important result, as it shows that the wavelength dependence of surface-plasmon scattering differs from that of photon scattering and that it can still be understood and described well with a simple expression.

The scattering cross sections that we measure are surprisingly large. The data presented in Fig. 5(a) correspond to $\xi = 36 \pm 13$, whereas theory predicts $\xi = 0.24$ for a simplified geometry [18]. There are several reasons for this discrepancy. First of all, the mentioned theoretical value was derived for a metal-air interface. By adapting the theory to a metal-glass interface, we predict that Eq. (4) should be multiplied by $n^6 = 11.9$, with n the refractive index of glass (see appendix A), thereby increasing the theoretical expectation to $\xi = 2.8$. The equations presented above automatically include this scaling when $k = 2\pi/\lambda = 2\pi n/\lambda_0$ in interpreted as the *wave number in the medium* and use $d_{spp} \approx \sqrt{\varepsilon}/(2n^2 k_0)$. Secondly, this value was derived for a perfect-electrical-conductor slab of zero thickness. The field penetration into the metal can increase the

#203316 - $15.00 USD Received 17 Dec 2013; revised 14 Feb 2014; accepted 17 Feb 2014; published 22 Apr 2014

effective hole radius by ~ 15 nm, thereby increasing a^6 by another factor ~ 3, making $\xi \sim 9$. But even this number is only a rough approximation. There is no real theory for our glass-metal-air geometry, which includes two dielectrics and a lossy metal of finite thickness, and the mentioned n^6 scaling only applies to a metal film that is fully embedded by a single dielectric. Hence, the quantitative difference between experiment and theory does not worry us too much. For now, we are only interested in the wavelength dependence of the cross section. The factor ξ is just a constant in the Rayleigh limit, albeit a complicated constant that depends crucially on the geometry and material composition of the hole and its surroundings.

Our technique is sensitive enough to observe a gradual changes in the structure. For this, we compare the results presented in this paper with the single-wavelength results presented in [25]. The later results were obtained with the same method and on the same sample, but one year before the current measurements. During that year, the scattering cross section at $\lambda = 740$ nm has almost doubled from the value $\sigma \approx$ 36 nm (= intensity cross section = $2\times$ amplitude cross section reported in [25]) to the value $\sigma \approx 60$ nm that we now find. At the same time, the average transmission of the random-hole patterns increased by a factor $\sim 3\times$, while SEM images show that the average hole size has increased from the original radius $a = 60$ nm to a new radius $a =$ 70 nm. Our observation that the absorption loss remains unchanged, and in agreement with literature values, indicates that the changes occur in the geometry rather than in the quality of the metal-glass interface. Metal films are known to change in time, but aging is typically observed at elevated temperatures. Our measurements indicate that phenomena such as diffusion of chromium in gold [37] and grain growth and grain boundary migration [38] could also be important at room temperature, at least if one waits long enough. A systematic study of these dynamic processes is difficult though, as they typically depend crucially on growth conditions, such as deposition rate and substrate temperature [37]. Fortunately, the precise composition of the film only shows up in the pre-factor ξ and has no effect on the studied wavelength dependence of the scattering cross sections.

4. Intensity-ratio cross section $A = \eta\sigma_{spp}$

Next, we consider the intensity-ratio cross section A and its wavelength dependence. In Fig. 5(b) we plot the extracted value for A as a function of wavelength. A spans roughly an order of magnitude and is of comparable magnitude as σ, suggesting that A and σ may be related. Similar to σ, A has a stronger wavelength dependence than λ^{-4}. At sufficiently large wavelength, where $d_{spp} \propto k^{-2}$, we expect $A \propto \sigma_{spp} \propto k^7$.

In appendices A and B, we will show that the intensity-ratio cross section $A = \eta\sigma_{spp}$, where σ_{spp} is the cross section from scattering of surface plasmons into other surface plasmons, instead of photons. The efficiency η describes, for an incident surface plasmon, how much power is radiated into the substrate relative to the total power scattered out at this hole. When these scattering processes are mediated via the same (magnetic) dipole moment, we also find $A/\sigma = \eta\sigma/\sigma_{spp} = \eta(3\lambda/16d_{spp})$, where $\lambda = \lambda_0/n$.

In Fig. 5(b) we plot a fit of $A = \eta\sigma(3\lambda/16d_{spp})$, using the efficiency η as the only

#203316 - $15.00 USD Received 17 Dec 2013; revised 14 Feb 2014; accepted 17 Feb 2014; published 22 Apr 2014

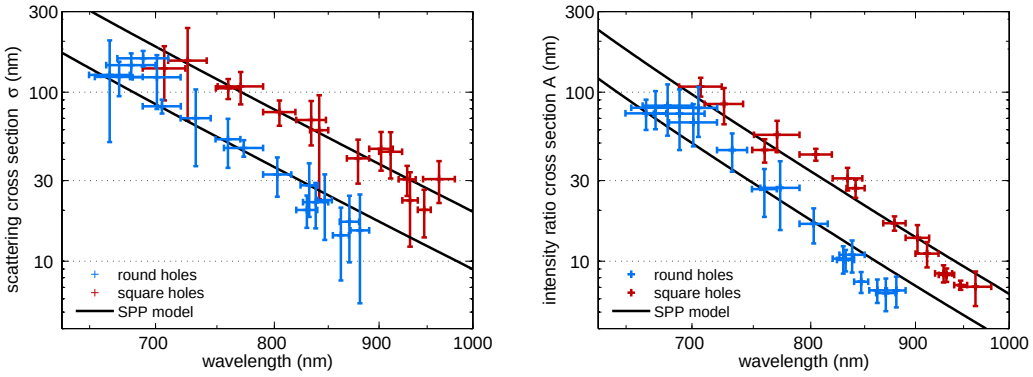

Fig. 6. (a, left) The measured values of the scattering cross section σ for circular and square holes. For both types, the predicted wavelength dependence reproduces the data accurately. The pre-factor for the round holes is smaller however. (b, right) The measured values of the intensity-ratio cross section A for round and square holes. Also for this parameter the predicted wavelength dependence describes the data of both round and square holes.

free parameter. We used scattering cross sections σ calculated from the fit from Fig. 5(a) to limit the noise. We obtain a fitted value of $\eta = 0.67 \pm 0.19$, which is reasonable as we expect this efficiency to be close to, but smaller than, one. This demonstrates the consistency of the experimental data and the data analysis. We are able to relate two independent quantities (the intensity ratio and the spectral width) to the same scattering cross section σ, using a simple efficiency factor η.

5. Results for square holes

The results presented so far were obtained for random patterns of circular hole, with a diameter of $2a = 140 \pm 8$ nm. We have also performed similar measurements on random patterns of square holes with side length 151 ± 6 nm. We are interested whether the shape has any influence on the magnitude of the scattering cross section and its wavelength dependence.

In Fig. 6(a) we plot the results for the scattering cross section of the square holes, along with the results for the round holes presented earlier. The measured scattering cross section σ is larger for the square hole than that of the round holes, but its wavelength dependence is very similar. The suggested wavelength dependence $\sigma = \xi k^4 a^6 / d_{spp}$ accurately fits the experimental data, where we choose a the rib length divided by two. The pre-factor ξ is found to be 1.7 ± 1.3 larger for the square holes.

In Fig. 6(b) we plot the results for the intensity-ratio cross section, also with the results of the round holes. The value of A is larger for the square holes too. We fit the expected wavelength dependence of $A = \eta\sigma(3\lambda/16d_{ssp})$, using the value of ξ just found and leaving only η as a free parameter. We thus find $\eta = 0.60 \pm 0.13$, which is comparable to that of round holes.

In conclusion, the data for the square hole shows the same wavelength dependence

#203316 - $15.00 USD Received 17 Dec 2013; revised 14 Feb 2014; accepted 17 Feb 2014; published 22 Apr 2014

of σ and A. The pre-factors η and ξ obtained for the square holes do not differ significantly from those found for round holes.

6. Conclusions

The scattering cross section of surface plasmons scattered by a sub-wavelength hole is measured in the wavelength range of 650-900 nm. The reported wavelength dependence is stronger than Rayleigh scattering predicts, because a surface plasmon polarizes the hole less efficiently at larger wavelengths. Nonetheless, this behavior can be captured in a simple expression.

Additionally, the measured scattering cross section explains the ratio between surface plasmon-mediated transmission and direct transmission of random hole patterns. Our results therefore imply that it may be viable to model particular complex plasmonic structures, like metal hole arrays, using only physical parameters like the hole size, hole density and film thickness. The magnitude of the measured scattering cross section is surprisingly large in comparison with recent theoretical predictions.

The presented methodology of obtaining scattering cross sections from transmission measurements on samples of different hole densities is surprisingly powerful, and may prove to be fruitful outside plasmonics too. Moreover, we showed the advantage of using random patterns instead of arrays, as the randomness allows measurements at virtually any wavelength without changing the illumination angle and thus the character of the excited dipole moments.

Appendix A: Relating model parameters to polarizability

In this Appendix, we will briefly discuss a recent calculation of the scattering cross section of surface plasmons from a single hole in a metal film, presented as supplementary material to [18]. This calculation starts from an incident surface plasmon on a metal dielectric interface, of which the power per unit length $P/L_\perp$ is calculated. Next, the hole in the metal is treated as polarizable object, which is polarized relative to its surroundings, with an induced (dominantly vertical) electric dipole $p = \alpha_E E$ and horizontal magnetic dipole $m = \alpha_M H$, where E and H are the electric and magnetic field component of the incident surface plasmon, respectively. Finally, the authors calculate the field emitted by these induced dipoles, assuming an otherwise smooth film, and thereby the power scattered to free space P_{out} and to the surface plasmon field P_{spp}. The associated scattering cross sections σ and σ_{spp} are found after division by the power per unit length $P/L_\perp$ [18]:

$$\sigma = \frac{P_{out}}{P/L_\perp} \approx \frac{32\pi k_0^5}{3\sqrt{|\varepsilon|}}(|\alpha_E|^2 + |\alpha_M|^2) \tag{5}$$

$$\sigma_{spp} = \frac{P_{spp}}{P/L_\perp} \approx \frac{8\pi^2 k_0^5}{|\varepsilon|}(2|\alpha_E|^2 + |\alpha_M|^2) \tag{6}$$

The polarizabilities α_E and α_M follow from a modal expansion of the EM field in cylindrical waves by imposing field continuity at the material boundaries, but this cal-

#203316 - $15.00 USD Received 17 Dec 2013; revised 14 Feb 2014; accepted 17 Feb 2014; published 22 Apr 2014

culation is difficult. The theoretical results presented in [18] show that each polarizability scale as a^3, where a is the hole radius, multiplied by a dimensionless factor that is constant for $a/\lambda \ll 1$. The magnetic polarizability α_M exhibits a shape resonance around $a/\lambda \approx 0.2$ and decreases for larger a/λ. The electric polarizability is almost a factor two smaller for $a/\lambda \ll 1$ and exhibits no resonance but simply decreases for larger a/λ. The polarizability of an infinitely thick film is predicted to be somewhat smaller than that of a film with a zero thickness film. For the calculations in the main text, we used the zero thickness values $\alpha_M = 0.106\, a^3$ and $\alpha_E = 0.054\, a^3$, which yields $\xi \approx 0.24$ in the expression $\sigma = \xi k^4 a^6 / d_{spp}$.

For completeness we note that the electric and magnetic response of single subwavelength holes have also been measured recently by Rotenberg et al. [39]. From the optical field observed close to an illuminated hole they were able to deduce the strength and angle-dependence of the surface plasmon to surface plasmon scattering. The magnetic polarizability α_M that they find is approximately as expected, but the measured electric polarizability α_E is larger than expected and about as large as α_M.

In the main text, we have rewritten Eq. (5) in terms of the mode size of the surface plasmon $d_{spp} \approx \sqrt{|\varepsilon|}/(2k_0)$ to stress that the induced dipole should be proportional to the incident field and scale as $\propto 1/\sqrt{d_{spp}}$. This removes the factor $\sqrt{|\varepsilon|}$ from the denominator and allows us to write $\sigma = \xi k^4 a^6 / d_{spp}$ for the scattering cross section of surface plasmons to photons. The power radiated to the surface plasmon field contains another factor $\lambda / d_{spp} \propto 1/\sqrt{|\varepsilon|}$ to account for the 'width of the angular spectrum of the surface plasmon' [40].

The theory in [18] assumes that the surface plasmon exists on a metal-air interface. In our experiment, however, it exists on a gold-glass interface. This modifies the expressions. For Rayleigh scattering, we expect that the factor k_0^4 should be replaced by k^4, with $k = nk_0$ as the wave vector inside the medium [41]. As the expression for the mode size $d_{spp} \approx \sqrt{\varepsilon}/(2n^2 k_0)$ contains the refractive index squared, we predict that the scattering cross section $\sigma \propto n^6$.

Division of Equation (6) by (5) yields the elegant result:

$$\frac{\sigma_{spp}}{\sigma} = \frac{(\lambda/d_{spp}^2)\,\pi k_0^4 \left(2|\alpha_E|^2 + |\alpha_M|^2\right)}{(1/d_{spp})\,(16/3)\pi k_0^4 \left(|\alpha_E|^2 + |\alpha_M|^2\right)} = \frac{3\lambda}{16 d_{spp}} \frac{2|\alpha_E|^2 + |\alpha_M|^2}{|\alpha_E|^2 + |\alpha_M|^2}, \qquad (7)$$

where the wavelength $\lambda \equiv \lambda_0/n$. If the magnetic polarizability dominates over the electric polarizability, the ratio between these two cross sections is $\sigma_{spp}/\sigma \approx (3\lambda/16 d_{spp})$. For the more realistic case $|\alpha_M/\alpha_E| = 2$, $\sigma_{spp}/\sigma \approx 1.2 \times (3\lambda/16 d_{spp})$. This ratio is equal to the power radiated to the surface plasmon field relative to that radiated to free space. It is also equal to the density of modes of the surface plasmon field relative to that of the free space modes. This ratio is approximately 0.5 for gold at 800 nm.

Appendix B: Intensity-ratio cross section $A = \eta\, \sigma_{spp}$

In this Appendix, we relate the intensity-ratio cross section A, extracted from our measurements, to the scattering cross section σ_{spp}. We do this by considering the power

#203316 - $15.00 USD Received 17 Dec 2013; revised 14 Feb 2014; accepted 17 Feb 2014; published 22 Apr 2014

flow depicted in Fig. 7, which is linked to the power flow in our experiment by the principle of reciprocity. We consider an incident plane wave with power P_{in}, which polarizes a hole on the glass side of the gold film. The induced dipole will radiate power into three channels: P_d into the substrate, P_{spp} into the surface plasmon field, and P_1' back into the waveguide (not shown). The surface plasmon field is then either absorbed or scattered as photons, into the substrate (power P_2) or into the waveguide (power P_1). The corresponding loss rates for these processes are the rates L_{abs}^{-1} and $\sigma\rho$ mentioned in the main text, making $(P_1+P_2)/P_3 = \sigma\rho/(L_{abs}^{-1}+\sigma\rho)$, a ratio that approaches one in the high-density limit where radiative loss dominates. Combination of these expressions now yields the intensity ratio of the surface-plasmon-mediated transmission over the direct transmission

$$\frac{\langle I_s\rangle}{\langle I_d\rangle} \equiv \frac{P_2}{P_d} = \frac{P_{spp}}{P_d}\,\frac{\sigma\rho}{L_{abs}^{-1}+\sigma\rho}\,\frac{P_2}{P_1+P_2} = \eta\,\frac{\sigma_{spp}\rho}{L_{abs}^{-1}+\sigma\rho}\,, \tag{8}$$

where we introduced the efficiency $\eta = P_2/(P_1+P_2)$, to quantify how much of the out-coupling is to the substrate relative to all light scattered out, and used $P_{spp}/P_d = \sigma_{spp}/\sigma$. A comparison with Eq. (3) from the main text immediately shows that the intensity-ratio cross section $A = \eta\sigma_{spp}$.

This is a very important result as it shows that the intensity-ratio cross section A is closely related to the scattering cross section of surface plasmons into other surface plasmons. We expect η to be smaller but close to one, making A just a little bit smaller than σ_{spp}. The measured ratio

$$\frac{A}{\sigma} = \eta\,\frac{\sigma_{spp}}{\sigma} = \eta\,\frac{3\lambda_0/n}{16 d_{spp}}\,, \tag{9}$$

thus enables us to simultaneously check the validity of (i) our expression for the ratio of the scattering cross sections σ_{spp}/σ and (ii) our assumption that the magnetic dipole dominates over the electric dipole. Under this assumption, theory and experiment provides a good match for the reasonable efficiency $\eta \approx 0.69 \pm 0.19$ mentioned in the main text.

We finally return to the correlation function C, which can be written as

$$C = \frac{\langle I_d\rangle^2}{\langle I_d+I_s\rangle^2}\left|1+\frac{A\rho}{\sigma\rho+L_{\mathrm{abs}}^{-1}-i\,\mathrm{Re}\,[\Delta k_{\mathrm{spp}}]}\right|^2, \tag{10}$$

after insertion of Eqs. (2) and (3) into Eq. (1). The theory presented above yields expressions for all quantities in the above expression. The most important ones are the scattering cross section $\sigma = \xi k^4 a^6/d_{spp}$, the intensity-ratio cross section $A = \eta\sigma_{spp} = \eta\sigma(3\lambda/16 d_{ssp})$ (for dominant magnetic dipoles), and the absorption length L_{abs}. These can in principle be calculated from the hole size a (and its geometry), the optical wavelength λ, and the metal properties. The ratio $\langle I_d\rangle^2/\langle I_d+I_s\rangle^2$ simply normalizes the result. The presented description is an important step forward in understanding random patterns in terms of their relevant design parameters. The next challenge will be

#203316 - $15.00 USD Received 17 Dec 2013; revised 14 Feb 2014; accepted 17 Feb 2014; published 22 Apr 2014

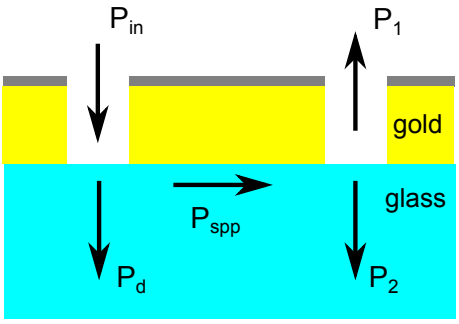

Fig. 7. Sketch of the power flow in our sample. An incident plane wave with power P_{in} induces a dipole moment. This dipole radiates into three channels: through the hole (P_1', not shown), into the substrate (P_d) and to a surface plasmon mode P_{spp}. The surface plasmon field is then either absorbed or scattered as photons, into the substrate (power P_2) or into the waveguide (power P_1).

to better understand the dimensionless quantities ξ and η in the expressions for σ and A.

Acknowledgements

We acknowledge M.J.A. de Dood and M. Orrit for discussions. This work is part of the research program of the Foundation for Fundamental Research on Matter (FOM), which is part of the Netherlands Organisation for Scientific Research (NWO).